Post-Print

This is the accepted version of:

S.C. Gibbs, S. Fichera, A. Zanotti, S. Ricci, E.H. Dowell
Flow Field Around the Flapping Flag
Journal of Fluids and Structures, Vol. 48, 2014, p. 507-513
doi:10.1016/j.jfluidstructs.2014.02.011

The final publication is available at https://doi.org/10.1016/j.jfluidstructs.2014.02.011

Access to the published version may require subscription.

When citing this work, cite the original published paper.

Flow field around the flapping flag

S.C. Gibbs [a], Sebastiano Fichera [b], Alex Zanotti [b],
Sergio Ricci [b], Earl H. Dowell [a]

[a] Duke University, Durham, NC, 27708, USA
[b] Politecnico di Milano, Milan, Italy

Introduction

A cantilever plate with flow along its elastic axis exhibits a flutter instability when the flow velocity increases above a critical velocity. The structure then enters a large and violent Limit Cycle Oscillation (LCO) that depends on the non-linearities in the fluid and the elastic structure. The literature contains extensive explorations of this system, but a complete understanding of the dynamics, especially in the post-flutter LCO regime, remains elusive. Understanding the post-flutter response of the flapping flag is especially important in light of the applications of the phenomenon that include using a flapping flag for energy harvesting (Akcabay and Young, 2012; Doaré and Michelin, 2011; Dunnmon et al., 2011; Giacomello and Porfiri, 2011; Michelin and Doaré, 2013), autonomous vehicle propulsion (Eloy and Schouveiler, 2011; Hellum et al., 2011; Jafferis and Sturm, 2013), and as a way to explain human snoring (Balint and Lucey, 2005; Huang, 1995; Howell et al., 2009). Understanding the response of this system at velocities above the flutter velocity includes predicting the amplitude of the LCO and capturing a hysteresis loop that is observed in experimental studies (Dunnmon et al., 2011; Eloy et al., 2012; Gibbs et al.,

2012; Tang et al., 2003). A hysteresis loop is a non-linear phenomenon that describes a system whose response depends on its past states.
For the flapping flag, the hysteresis loop manifests itself in a range of flow velocities where it is possible to have either a stable or an unstable response depending on whether one is increasing or decreasing the flow velocity.
It is difficult to model the post-critical behavior of the system because non-linear effects cause both the LCO and the hysteresis. Many authors including Dunnmon et al. (2011), Eloy et al. (2012), Michelin et al. (2008) and Tang and Païdoussis (2007, 2008) have created non-linear models. Currently, the non-linear theoretical models of the flapping flag largely focus on non-linearities in the structural dynamics. For example, Tang et al. (2003) developed a theoretical model using a non-linear inextensible beam coupled to a linear three-dimensional vortex lattice aerodynamic model to predict the post- critical response. The theoretical predictions accurately predict the flutter boundary, but underestimate the LCO amplitude and do not capture the hysteresis loop. In general, aeroelastic models that include classical structural nonlinearities have not been able to predict accurately the LCO amplitude.
Aeroelastic models are usually based on both linear and nonlinear structural models combined with potential flow aerodynamic models. With advances in computational power, recent studies have also studied viscous effects by using CFD techniques to solve the Navier–Stokes equations (Balint and Lucey, 2005; Gordnier and Visbal, 2002; Watanabe et al., 2002). However, even with the advances in computational power, it is still not efficient to use these computational tools for three dimensional simulations and parameter variation studies. Furthermore experiments by Zhang et al. (2000) on a flexible filament in flowing soap films indicated that no flow separation occurs along the flexible body suggesting that viscous effects may not be important. Our current research complements the previous experimental work from Zhang et al. (2000) by looking at the flow around the flapping flag in air. This note presents flow visualization around the midspan of an elastic plate in air during a LCO using Particle Image Velocimetry (PIV) techniques. This research quantifies the flow field in a single plane during the LCO and suggests how researchers can improve fluid models to capture more accurately the aerodynamic features of the flow field. The note focuses on the experimental results for a single representative configuration. We observe no significant separation in the flow confirming the previous observations of Zhang et al. (2000), thus suggesting that viscous flow models may not be needed to improve the theoretical predictions for the flapping flag post-critical response.

Experimental methodology

The test article is a 275 mm by 151 mm piece of aluminum with the properties listed in Table 1. These parameters correspond to a mass ratio ($\rho_a Lx/\rho_s h$) of 0.305 and an aspect ratio (Ly/Lx) of 0.55. For this configuration, the literature (Eloy et al., 2008; Gibbs et al., 2012) suggests that the system will lose stability in a flutter mode that is a coalescence of the first and second elastic bending modes. A simulation done with the theoretical model from Gibbs et al. (2012) predicts a flutter instability at 24 m/s and 20 Hz. We validate the structural model by comparing the ground vibration experiment natural frequencies to theoretical predictions.
We conducted the aeroelastic experiment in the Politecnico di Milano Small Wind Tunnel (PSWT), a closed circuit low- speed wind tunnel, with a rectangular test section of 1.5 x 1 x 3 m and no heat exchangers installed. For the aeroelastic experiment, a rigid airfoil clamps the elastic

plate at its leading edge. The rigid airfoil is then mounted horizontally in the wind tunnel. This alignment differs from the vertical mounting in previous experiments, but is necessary to accommodate the PIV setup. Fig. 1 shows the actual experimental setup and Fig. 2 shows a schematic representation of the setup.
The PIV setup shown in Fig. 2 uses a double shutter CCD camera with a 12 bit, 1952 x 1112 pixel array and a 50 mm lens to acquire the image pairs. The setup uses a Nd:Yag double pulsed laser with 200 mJ output energy and a wavelength of 532 nm. The laser sheet passes through an opening in the wind tunnel roof aligned with the flow and positioned in the midspan of the experiment specimen.

Experimental Beam Properties.

Property	Symbol	Value
Density	ρ_s	2840 kg/m^3
Young's modulus	E	72 GPa
Thickness	h	0.381 mm
X Length	L_x	275 mm
Y Length	L_y	151 mm

Table 1

Fig. 1. Test specimen mounted in the wind tunnel in preparation for experiments.

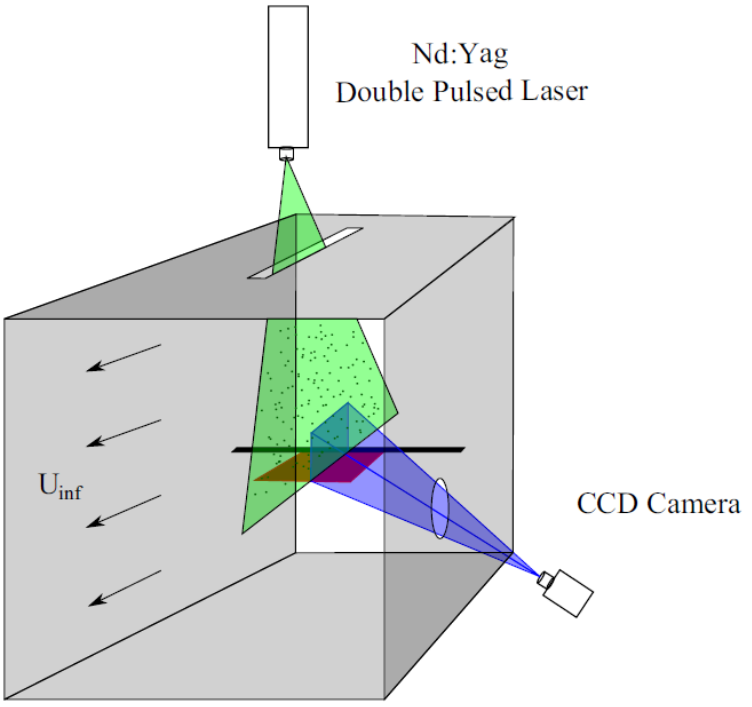

Fig. 2. Schematic of PIV wind tunnel setup.

Upper flutter velocity (m/s)	25.5
Lower flutter velocity (m/s)	24.0
LCO frequency(at 26 m/s)(Hz)	19.73

Table 2 Aeroelastic experiment results.

The laser and the camera are mounted on an external metallic structure made of aluminum profiles that are connected to the heavy basement in order to avoid the transfer of the wind tunnel vibrations to the PIV measurement devices during the tests. A particle generator with Laskin nozzles is used for the flow insemination. The tracer particles consist of small oil droplets with a diameter within the range of 1–2 μm. The particles are injected into a section just after the fans and fill the wind tunnel volume with homogeneous density. The image pairs post-processing is carried out using the PIVview 2C software (PIVTECH, 2013) of PIVTEC. Multigrid technique (Raffel et al., 1998) is employed to correlate the image pairs, up to an interrogation window of 64 64 pixels.

Table 2 contains the stability boundary results for the aeroelastic experiments. The precision was limited because we did not instrument the panel during the aeroelastic experiments in order to minimize aerodynamic disturbances in the flow. The experiment was conducted by slowly increasing the flow velocity until the system entered a LCO. We acquired the PIV snapshots at a velocity of 26 m/s, a velocity slightly above the flutter velocity, at a sample period selected to freeze the panel motion between snapshots, effectively identifying the frequency of the LCO. At this velocity, the LCO amplitude is about 1/2 of the streamwise length of the plate. After

collecting data, we reduced the flow velocity until the system returned to a stable state. As noted in the literature (Dunnmon et al., 2011; Eloy et al., 2012; Gibbs et al., 2012; Tang et al., 2003), the velocity where the system regains stability is lower than the velocity at which the system becomes unstable. For the experiment the Reynolds number is 2×10^5 and the LCO Strouhal number ($\omega Lx/U$) is 0.07.

Observations

For the experiments there are two types of PIV visualizations that are conducted. The first set uses images captured at the same phase of the flag oscillation and the second set includes images taken at different steps in a single period of the oscillation. The first set is used to analyze the phase average of the flow field. This is a common technique in PIV analyses to separate a flow into a mean and a fluctuating part. This is important because it allows researchers to identify turbulent structures in the flow. This type of measurement is important if we are to observe flow separation on the plate. The second type of experiment is useful for creating a visualization of how the flow changes during a single oscillation period. This is useful for producing visualizations of the flow evolution.

This note contains the phase averaged flow fields for two different times in the LCO. Fig. 3 shows the theoretical flutter mode shapes, the PIV viewing window and highlights the two flag shapes that we will analyze. Note that the mode shapes in Fig. 3 do not take into account the effect of the gravity that would lead to a slight up/down asymmetry. The first image set analyzed is taken at a moment when the point of the plate on the upstream boundary of the PIV viewing window is moving up and the trailing edge is moving down. The document will refer to this as the upstroke configuration.

Fig. 4 shows the phase-averaged flow-field in the upstroke. The fluid moves from right to left in the figure. The figure also contains streamlines seeded at the right-hand side of the image. The region with no streamlines is the location of the panel that is masked to avoid displaying confusing and physically irrelevant flow vectors.

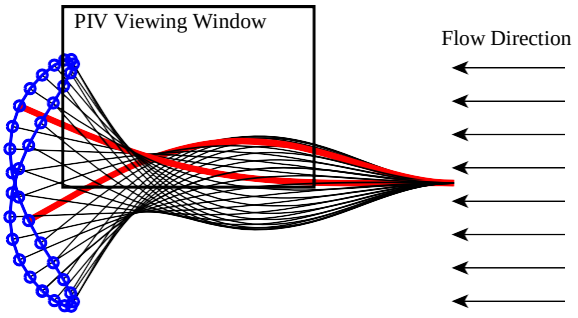

Fig. 3. Theoretical flutter mode shapes with PIV window identified.

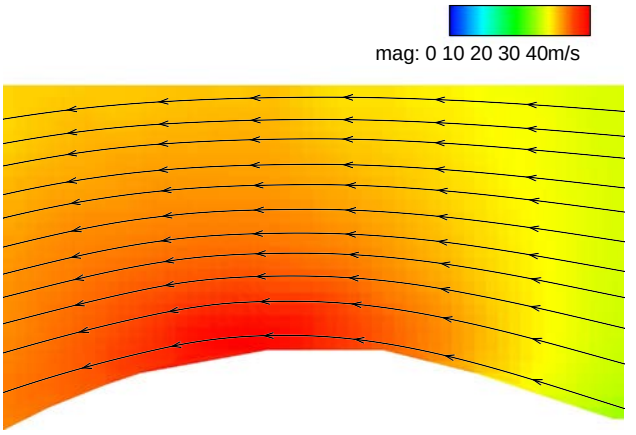

Fig. 4. Upstroke phase average flow-field with streamlines.

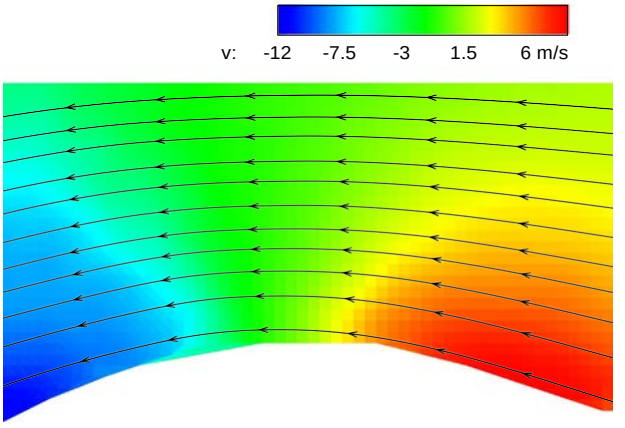

Fig. 5. Upstroke phase average vertical component of the flow-field.

Fig. 5 shows the vertical component of the velocity field. Fig. 5 clearly shows the flow following the upward motion of the front half of the plate and the downward motion of the back portion of the plate. The most striking feature of this analysis is that the flow is attached along the panel. According to the images the flow completely conforms to the structural motion with the streamlines following the local slope of the flapping flag. The streamlines also suggest that there is no inverse flow flux.

Fig. 4 shows no separation at this specific point in the oscillation, but it is possible that there could be other points in the limit cycle that are more critical. The second analysis explores snapshots taken when the point on the plate on the upstream boundary of the PIV viewing window is beginning to descend and the trailing edge is still moving in the upward direction. This portion of the oscillation is at the beginning of the downstroke. We choose this portion of the motion because the plate curves in the opposite direction to the first pair of images. Figs. 6 and 7 show the phase averaged flow field and phase averaged vertical component of the flow field respectively. As was the case previously, the streamlines in the figures suggest a fully attached flow with no flow separation.

Because the phase averages suggest that the flow is attached, we can select single snapshots

throughout the oscillation period and create a set of images that captures the fluid motion through a full period of the flag motion without needing to phase average every image. Fig. 8 shows snapshots from eight different times in the flag cycle. The figures progress left to right and top to bottom. The figures contain streamlines and the flow velocity. The figures confirm the benign and attached nature of the flow for this system, where at a given position the flow is conformal to the structural motion.

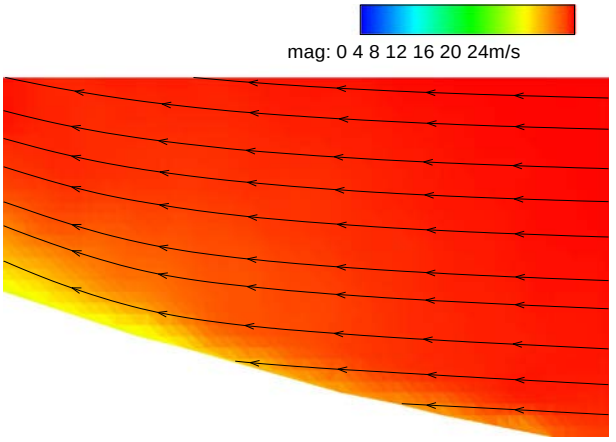

Fig. 6. Downstroke Phase Average Flow-field with Streamlines.

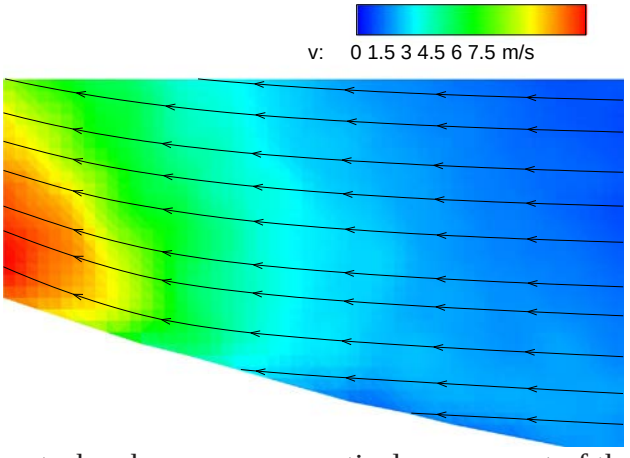

Fig. 7. Downstroke phase average vertical component of the flow-field.

Conclusions

This note presents experimental observations of the flow field around the midspan of the flapping flag while in a LCO. The flow fields are captured using typical PIV techniques and show that the flow remains attached to the flapping flag within the observation area, even while the structure is in a violent, large amplitude LCO. This observation has significant implications for the way that we model the aerodynamics in aeroelastic models of the system. Because the flow is attached and

well behaved, linear or nonlinear potential flow aerodynamic theories used in many of the flapping flag aeroelastic theories may be capable of accurately capturing the flow field seen in the experiment. Furthermore, for the case of heavy flags in light fluids, which corresponds to small mass ratios, including viscous effects by solving the Navier–Stokes equations may not be the best way to improve the theoretical predictions of the post-critical response. Instead, potential flow theories that are capable of capturing the large geometric deflections during the LCO may be adequate. An example of an applicable model would be to extend the linear vortex lattice model used by previous researchers to model nonlinear effects. An example of such a model is found in Attar (2003) where the vortex elements are shed at the trailing edge of the displaced structure into a free wake that is allowed to convect and move freely.

Our observations also suggest that continued improvements to the structural non-linear models may improve the agreement between theory and experiment for the post-critical response of the flapping flag. A particularly promising development from Tang et al. (submitted for publication) that includes non-linear inertia effects shows promise in matching limit cycle oscillation amplitude theoretical predictions to experimental measurements.

Finally, there are additional visualizations that would be an interesting avenue for future research. Due to the camera's view field limitations, we focused on capturing the flow over the plate so that we could identify regions of flow separation. With additional time and resources, one could investigate the wake behind the plate to explore any large wake structures that are formed during the LCO. The current study is also limited to exploring the flow in a single plane over the midspan of the flapping flag. Exploring the flow field in a plane transverse to the flow as well as locations near the edges of the plate could identify strong 3D aerodynamic effects and further strengthen the conclusions of the current study.

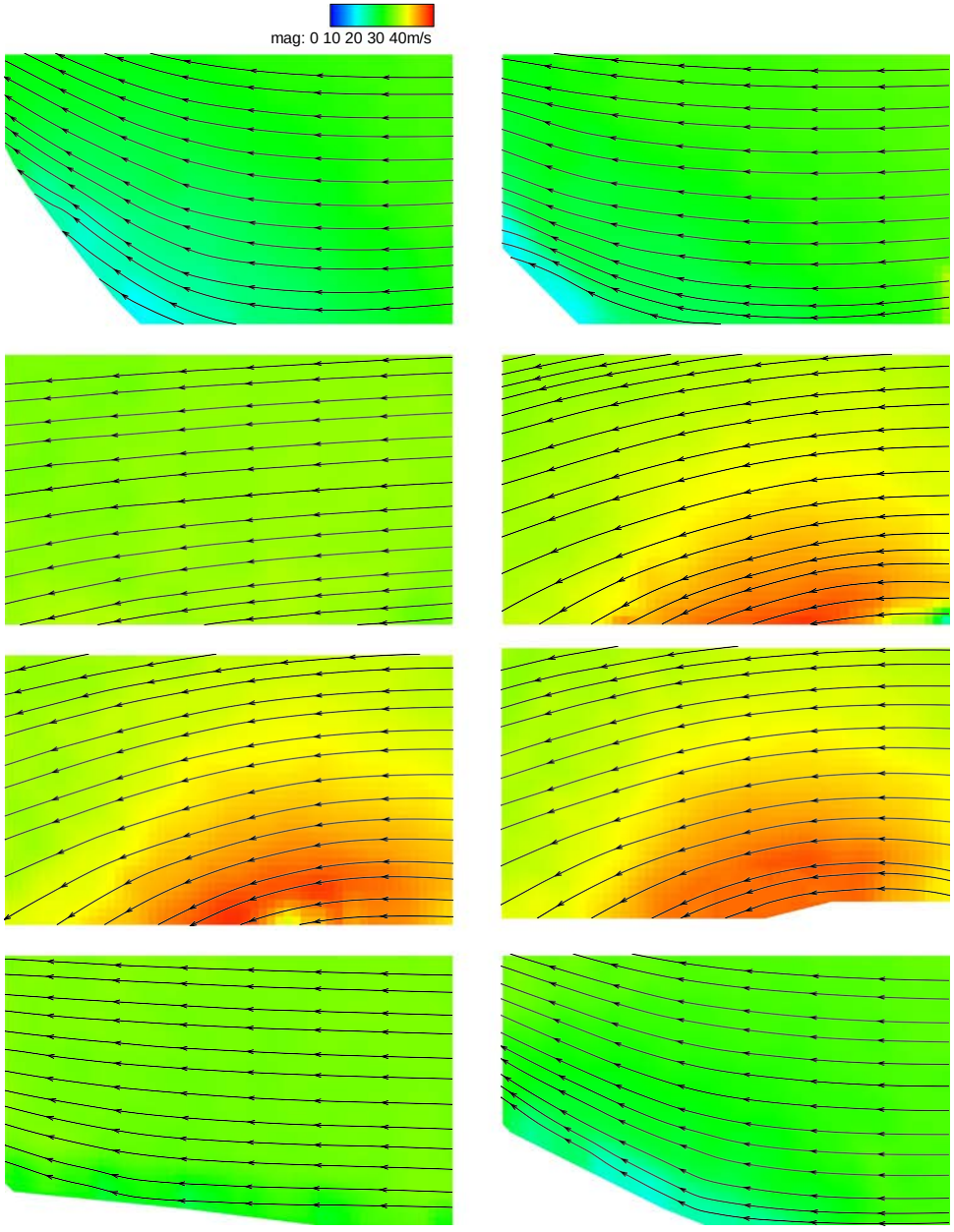

Fig. 8. Snapshots from different phases in the LCO with streamlines.

References

Akcabay, D.T., Young, Y.L., 2012. Hydroelastic response and energy harvesting potential of flexible piezoelectric beams in viscous flow. Physics of Fluids 24, 054106.

Attar, P., 2003. Experimental and Theoretical Studies in Nonlinear Aeroelasticity (Ph.D. thesis). Duke University.

Balint, T., Lucey, A., 2005. Instability of a cantilevered flexible plate in viscous channel flow. Journal of Fluids and Structures 20 (7), 893–912.

Doaré, O., Michelin, S., 2011. Piezoelectric coupling in energy-harvesting fluttering flexible

plates: linear stability analysis and conversion efficiency. Journal of Fluids and Structures 27 (8), 1357–1375.
Dunnmon, J., Stanton, S., Mann, B., Dowell, E., 2011. Power extraction from aeroelastic limit cycle oscillations. Journal of Fluids and Structures 27 (8), 1182–1198.
Eloy, C., Kofman, N., Schouveiler, L., 2012. The origin of hysteresis in the flag instability. Journal of Fluid Mechanics 691, 583.
Eloy, C., Lagrange, R., Souilliez, C., Schouveiler, L., et al., 2008. Aeroelastic instability of cantilevered flexible plates in uniform flow. Journal of Fluid Mechanics 611, 97–106.
Eloy, C., Schouveiler, L., 2011. Optimisation of two-dimensional undulatory swimming at high reynolds number. International Journal of Non-Linear Mechanics 46 (4), 568–576.
Giacomello, A., Porfiri, M., 2011. Energy harvesting from flutter instabilities of heavy flags in water through ionic polymer metal composites. In: Proceedings of SPIE, vol. 7976. p. 797608.
Gibbs IV, S.C., Wang, I., Dowell, E., 2012. Theory and experiment for flutter of a rectangular plate with a fixed leading edge in three-dimensional axial flow.
Journal of Fluids and Structures 34, 68–83.
Gordnier, R.E., Visbal, M.R., 2002. Development of a three-dimensional viscous aeroelastic solver for nonlinear panel flutter. Journal of Fluids and Structures 16 (4), 497–527.
Hellum, A., Mukherjee, R., Hull, A., 2011. Flutter instability of a fluid-conveying fluid-immersed pipe affixed to a rigid body. Journal of Fluids and Structures 27 (7), 1086–1096.
Howell, R., Lucey, A., Carpenter, P., Pitman, M., 2009. Interaction between a cantilevered-free flexible plate and ideal flow. Journal of Fluids and Structures 25 (3), 544–566.
Huang, L., 1995. Flutter of cantilevered plates in axial flow. Journal of Fluids and Structures 9 (2), 127–147.
Jafferis, N.T., Sturm, J.C., 2013. Fundamental and experimental conditions for the realization of traveling-wave-induced aerodynamic propulsive forces by piezoelectrically deformed plastic substrates. Journal of Microelectromechanical Systems 22 (2), 495.
Michelin, S., Doaré, O., 2013. Energy harvesting efficiency of piezoelectric flags in axial flows. Journal of Fluid Mechanics 714, 489–504. Michelin, S., Llewellyn Smith, S., Glover, B., 2008. Vortex shedding model of a flapping flag. Journal of Fluid Mechanics 617, 1–10.
PIVTECH, 2013. Pivview 2c Version 3.2, User Manual. URL: ⟨www.pivtec.com⟩.
Raffel, M., Willert, C.E., Kompenhans, J., 1998. Particle Image Velocimetry: A Practical Guide; with 24 Tables, Springer.
Tang, D., Yamamoto, H., Dowell, E., 2003. Flutter and limit cycle oscillations of two-dimensional panels in three-dimensional axial flow. Journal of Fluids and Structures 17 (2), 225–242.
Tang, D.M., Gibbs, S.C., Dowell, E.H., Theoretical and experimental aeroelastic flapping flag response: correlation with inextensible beam theory. Journal of Fluids and Structures, submitted for publication.
Tang, L., Païdoussis, M., 2007. On the instability and the post-critical behaviour of two-dimensional cantilevered flexible plates in axial flow. Journal of Sound and Vibration 305 (1-2), 97–115.
Tang, L., Païdoussis, M., 2008. The influence of the wake on the stability of cantilevered flexible plates in axial flow. Journal of Sound and Vibration 310 (3), 512–526.
Watanabe, Y., Isogai, K., Suzuki, S., Sugihara, M., 2002. A theoretical study of paper flutter. Journal of Fluids and Structures 16 (4), 543–560.
Zhang, J., Childress, S., Libchaber, A., Shelley, M., 2000. Flexible filaments in a flowing soap film as a model for one-dimensional flags in a two-dimensional wind. Nature 408 (6814), 835–839.